

Individualized Design of the Ventilator Mask based on the Residual Concentration of CO₂

Zhiguo Zhang^{1, *}, Zhenxiao Li², Yifei Zhang³, Zhenze Wang⁴ and Minzhou Luo¹

Abstract: OSAHS (Obstructive Sleep Apnea Hypopnea Syndrome) is a respiratory disease mainly characterized by limited and repeated pauses of breathing in sleep. Currently, the optimal treatment is to apply CPAP (Continuous Positive Airway Pressure) ventilation on the upper airway of the patient through a household respiratory machine. However, if the ventilator mask is designed improperly, it might cause the residue and repeated inhalation of CO₂, which will exert an adverse impact on the therapeutic effect. Present research numerically analyzed the CO₂ transportation inside a commercial ventilator mask (Mirage SoftGel, ResMed, Australia) based on the reconstructed 3D numerical model of a volunteer's face and performed the improved design of the ventilator mask in terms of the CO₂ residual concentration below the nostrils. The fluid dynamic analyses showed that at the end time of expiratory, the CO₂ residual concentration below the nostrils is close to 4%. To improve the therapeutic effect, we changed the position of the exhaust holes and found that by moving the exhaust holes to the bottom of the ventilator mask, the CO₂ residual concentration below the nostrils would be reduced to no more than 1%. This study established a near physiological computational model and provided a new method for the individualized design of the commercial ventilator mask.

Keywords: Obstructive sleep apnea hypopnea syndrome, continuous positive airway pressure, ventilator mask, CO₂ residual concentration, 3D numerical reconstruction.

1 Introduction

Severe snoring is often associated with obstructive sleep apnea hypopnea syndrome (OSAHS), which is mainly characterized by limited and repeated pauses of breathing and can lead to hypoxemia, hypercapnia, and memory deterioration [Liu, Lowe, Fleetham et

¹ Jiangsu Key Laboratory of Special Robot Technology, College of Mechanical and Electrical Engineering, Hohai University, No. 200. Jinling North Road, Xinbei, Changzhou, 213022, China.

² School of Mechanical Engineering, Changzhou University, No. 1. Gehu Road, Wujin, Changzhou, 213164, China.

³ School of Mathematics & Physics, Changzhou University, No. 1. Gehu Road, Wujin, Changzhou, 213164, China.

⁴ National Research Center for Rehabilitation Technical Aids, Beijing Key Laboratory of Rehabilitation Technical Aids for Old-Age Disability, Key Laboratory of Rehabilitation Technical Aids Technology and System of the Ministry of Civil Affairs, No. 1. Ronghuazhong Road, Beijing BDA, Beijing, 100176, China.

* Corresponding Author: Zhiguo Zhang. Email: zhangzg@cczu.edu.cn.

al. (2001); Chirapapaisan, Likitgorn, Pleumchitchom et al. (2016)]. Recent clinical studies show that OSAHS is correlated with the morbidity of diabetes and hypertension, which might lead to cardiovascular and cerebrovascular diseases [Shen, Tan, Song et al. (2017); Sun, Li and Shi (2016); Kim, Choi, Bail et al. (2013); Korcarz, Stein, Peppard et al. (2014)]. So far, main treatments for OSAHS include surgical treatment, oral appliance therapy and continuous positive airway pressure (CPAP) ventilation [Vecchierini, Attali, Collet et al. (2016)]. Because surgical treatment may relapse or lead to surgical complications, and oral appliance has adverse effects such as mandibular ache, mandibular arthritis or periodontal diseases [Rose, Staats, Virchow et al. (2002); Li (2005)], the non-invasive mechanical CPAP treatment is the major option for OSAHS patients, which can immediately alleviate the symptoms of limited breathing and significantly improve the sleep quality [Buchanan and Grunstein (2011); Mcevoy, Antic, Heeley et al. (2016)]. During CPAP treatment, ventilator mask plays a critical role in O₂ inhalation and CO₂ exhalation. The improper design of the ventilator mask might result in the residual and repeated inhalation of CO₂, which is detrimental to the therapeutic effect [Lofaso, Brochard, Touchard et al. (1995)]. Clinical data show that if the CO₂ concentration constantly inhaled by human exceeds 2%, there will be a headache, cardioacceleration or nausea. If it exceeds 4%, breath will become faster. If it exceeds 5%, it may lead to severe hypoxia, permanent cerebral injury, coma or even death [George and Daniel (2001)]. Therefore, proper design of the ventilator mask is directly related to the therapeutic effect of OSAHS and has very important significance.

Various studies measured the CO₂ concentrations in medical ventilator masks or oral-nasal masks. Among them, the side stream method (SideStream Spirometry) is a major one. By this method, Mediano et al. [Mediano, Garciaro and Villasante (2006)] compared 3 different medical ventilator masks in terms of repeated CO₂ inhalation during CPAP treatment; Peng et al. [Peng, Wang and Zhang (2005)] compared the impact of 3 different exhalation valves on the repeated inhalation of CO₂; Huang et al. [Huang, Wang and Tan (2015)] monitored the partial pressure of CO₂ inside the oral-nasal mask in a lung drive model (spontaneous breathing movements established). However, the limitation of the side stream method lies in that the catheter stretched into the mask would disturb the internal flow field and affect the measurement results of the local CO₂ concentration. Therefore, numerical simulations become the most important alternatives. Nevertheless, there are few studies on the ventilator masks of household CPAP machines. The existing studies are mainly focused on medical nasal masks or oral-nasal masks. Even so, these numerical models are over simplified. Such as Chen [Chen (2011)] only reconstructed a 3D numerical model of the mask without taking the patient's face into consideration. Their model was obviously an over-simplified one that could hardly reflect the real physiological condition.

In present study, a 3D numerical model of a volunteer's face integrated with the ventilator mask (Mirage SoftGel, ResMed, Australia) was built based on reverse engineering method. Then, the CO₂ transportation inside the ventilator mask under transient state was numerically analyzed with the boundary condition of nostrils. Finally, the improved design of the ventilator mask was performed based on the residual concentration of CO₂.

2 Materials and methods

2.1 Geometric model and the meshes

Firstly, the point cloud data of the ventilator mask (Mirage SoftGel, ResMed, Australia) and the face of the volunteer (male, 28 years old, OSAHS) were collected with the 3D laser scanner (HandySCAN700™, Creaform, Canada); then, the point cloud data were imported into the reverse engineering software (Geomagic Wrap) for post processing. The detailed steps were as follows: 1) Redundant point cloud data on the outside of the ventilator mask and the face were removed; 2) The point cloud data scanned from different directions were registered and combined into a whole for denoising; 3) The point cloud data were smoothed with the Mesh Doctor; 4) The results were imported into the Geomagic Design X to reconstruct the 3D numerical models of the ventilator mask and the volunteer's face; 5) The numerical models were imported into the ANSYS ICEM CFD 15.0 for meshing with the unstructured tetrahedral-hexahedral hybrid mesh. The obtained mesh models included about 375278 elements and 95042 nodes based on the mesh independence test; 6) The mesh models were imported into the ANSYS fluent 15.0 for CFD analysis (Fig. 1).

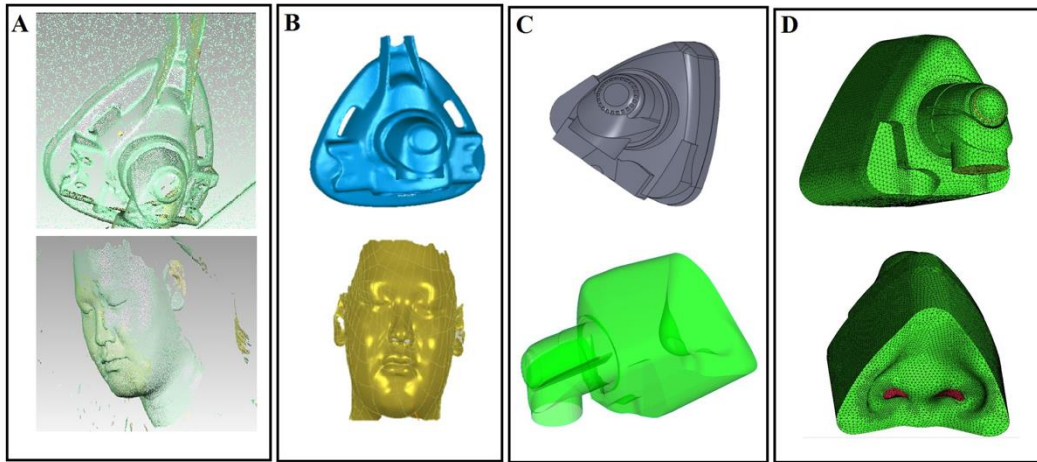


Figure 1: The reconstructed 3D numerical models of the ventilator mask (Mirage SoftGel, ResMed) and the face of the volunteer. A. The collected point cloud data; B. The fixed and encapsulated polygon model; C. The 3D numerical model of the ventilator mask integrated with the volunteer's face; D. The meshes

2.2 Governing equations

The air is assumed to be Newtonian and incompressible viscous fluid. The Navier-Stokes and mass transfer equations are as follows:

$$\nabla \cdot \mathbf{u} = 0 \quad (1)$$

$$\rho \frac{\partial \mathbf{u}}{\partial t} + \rho(\mathbf{u} \cdot \nabla)\mathbf{u} - \mu \nabla^2 \mathbf{u} + \nabla p = 0 \quad (2)$$

$$\frac{\partial c}{\partial t} - \psi \Delta c + \mathbf{u} \cdot \nabla c = 0 \quad (3)$$

where ρ , t , u , p , ψ , μ represents the density (kg/m^3), time (s), flow velocity (m/s), pressure (Pa), diffusion coefficient and kinetic viscosity, respectively. $\psi = 1.38 \times 10^{-5} m^2/s$, $\mu = 1.789 \times 10^{-5} N \cdot s/m^2$ [Calay, Kurujareon and Holdo (2002)].

2.3 Boundary conditions and solutions

- i. Inlet boundary condition at the entrance of the ventilator mask: The pressure $P_{in} = 0.98 \times 10^3 Pa$ [Wakayama, Suzuki and Tanuma (2016)]; the averaged concentration of CO₂ $\bar{M}_{CO_2} = 0.03\%$ [De Vis, Lu, Ravi et al. (2017)] (Fig. 2A);
- ii. Outlet boundary condition at the exhaust holes: $P_{out} = 0Pa$ (Fig. 2A);
- iii. Inlet boundary condition at the nostrils: The averaged velocity $\bar{U} = 6 \times \sin\left(\frac{\pi}{2} t\right)$, $t=0\sim 2.0$ s is the expiratory phase, $t=2.0\sim 4.0$ s is the inspiratory phase (Fig. 2B); the averaged concentration of CO₂ excreted from the nostrils is set as 4% [Zhu and Wang (2013)] and the CO₂ is inhaled freely in the inspiratory phase (Fig. 2C);
- iv. Rigid and non-slip wall boundary condition.

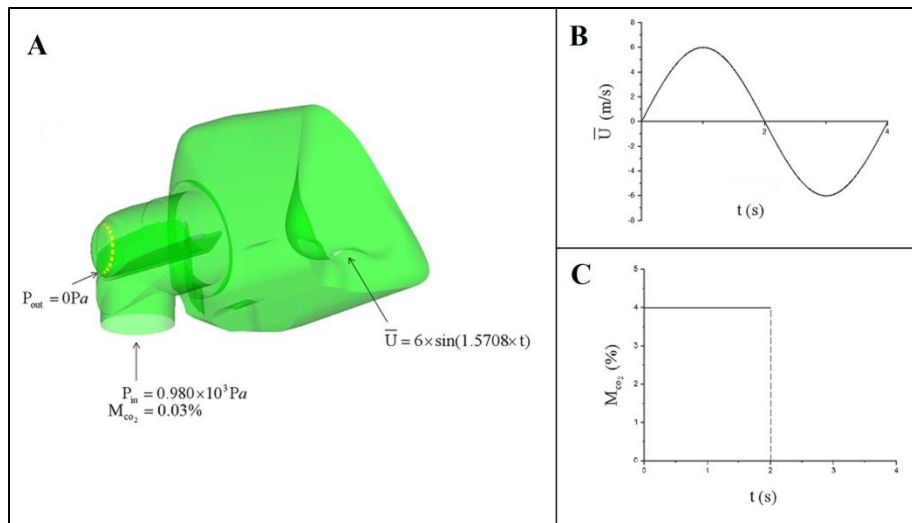


Figure 2: Boundary conditions: A. A schematic draw of the boundary conditions; B. Sinusoidal velocity inlet boundary condition at the volunteer’s nostrils; C. Plot of the averaged CO₂ concentration excreted from the nostrils in a respiratory cycle

The airflow inside the ventilator mask is assumed to be turbulent flow for the reason of the averaged Reynolds number at the inlet is approximately 4300 ($Re > 4000$) [Levitzyk (2007)]. The K- ϵ and Species models are used for computation. The software ANSYS fluent 15.0 is utilized for solving. The time step was set as 0.01 s.

3 Results and dicussion

3.1 Analysis of the CO₂ distributions inside the ventilator mask

Fig. 3 is the distribution of the \bar{M}_{CO_2} inside the ventilator mask varying with time during a respiratory cycle. The \bar{M}_{CO_2} rises dramatically with the increasing exhaled air and reaches the peak value of $\bar{M}_{CO_2} = 3.65\%$ at $t=1.1$ s. Then, with the decrease of the exhaled air, the \bar{M}_{CO_2} declines gradually and down to the value of 1.8% at the end time of expiratory ($t=2.0$ s). During the initial 0.5 s of the inspiratory phase, the \bar{M}_{CO_2} declines sharply and down to the initial value of 0.03%. It can be seen that the residual CO₂ is mainly dependent on the value of \bar{M}_{CO_2} at the end time of expiratory, which will be inhaled again.

Hence, the distribution of the residual CO₂ at the end expiratory time ($t=2.0$ s) was analyzed in detail. Fig. 4A is the schematic draw of the crosssection Y-Y' ($Y=7.5$ mm) and Z-Z' ($Z=75$ mm). Figs. 4B and 4C are the air velocity vector diagram and the cloud map of the CO₂ concentration on the crosssection of Y-Y', respectively. Figs. 5A and 5B is the air velocity vector diagram and the cloud map of the CO₂ concentration on the crosssection of Z-Z', respectively. It can be seen that due to the existence of the deflector, the inlet air firstly flows rapidly towards the inner and then flows towards the exhaust holes under the differential pressure (Fig. 4B). Meanwhile, the local vortices arise below the nostrils (Fig. 5A). Figs. 4C and 5B show that the \bar{M}_{CO_2} decreases to 1% in high velocity area and increases to 3% in low velocity vortex area.

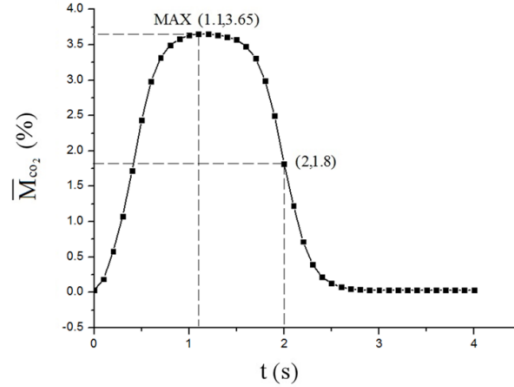


Figure 3: Distribution of the averaged residual CO₂ concentration inside the ventilator mask varying with time during a complete respiratory cycle. ($\bar{M}_{CO_2} = \frac{\sum M_i vol_i}{\sum vol_i}$, M_i represents the CO₂ concentration of the i th centroid, vol_i represents the volume of the i th centroid)

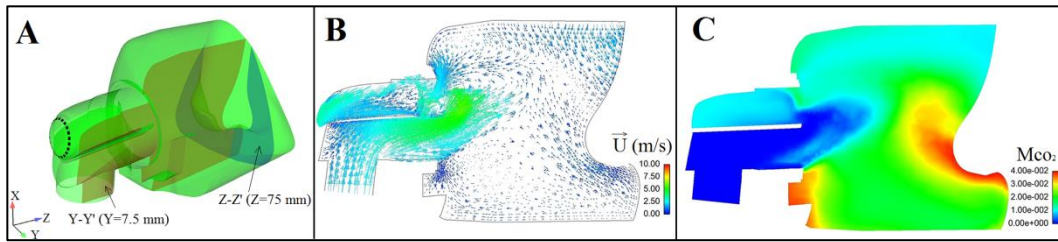


Figure 4: A. Schematic draw of the crosssection Y-Y' and Z-Z'; B. The velocity vector plot on the crosssection Y-Y' at t=2.0 s; C. The cloud map of the residual CO_2 concentration on the crosssection Y-Y' at t=2.0 s

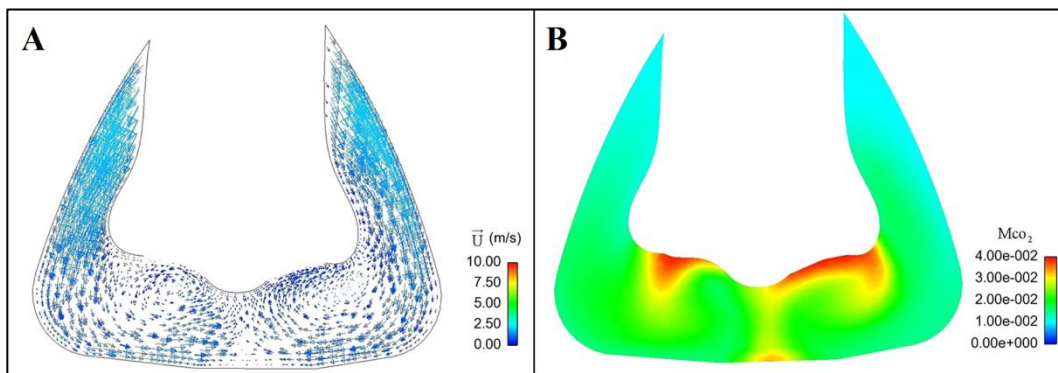


Figure 5: A. The velocity vector plot on the crosssection Z-Z' at t=2.0 s; B. The cloud map of the residual CO_2 concentration on the crosssection Z-Z' at t=2.0 s

3.2 Effects of the deflector on the averaged residual CO_2 concentration

Fig. 6A shows the geometric model of the ventilator mask without deflector. Because the inlet air flows directly towards the exhaust holes and large low velocity vortices arise below the nostrils (Fig. 6B), a great deal of CO_2 residues inside the mask with the value of \bar{M}_{CO_2} up to 4% (Fig. 6C).

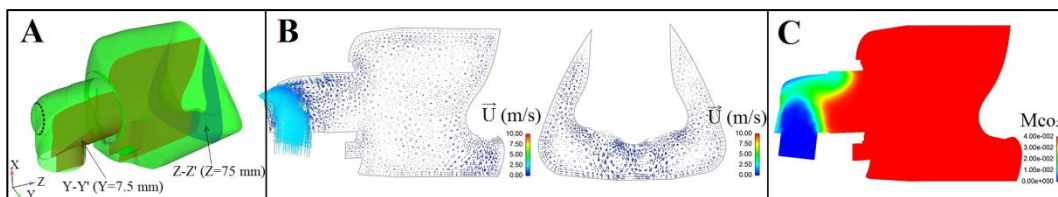


Figure 6: A. The geometric model of the ventilator mask without deflector; B. The velocity vector plots on the crosssection Y-Y' and Z-Z' at t=2.0 s; C. The cloud map of the residual CO_2 concentration on the crosssection Y-Y' at t=2.0 s

Fig. 7 is the distributions of the \bar{M}_{CO_2} inside the ventilator mask varying with time with/without deflector. It can be drawn that the \bar{M}_{CO_2} without a deflector is higher than

that with a deflector. At the end time of expiratory ($t=2.0$ s), the value of the \bar{M}_{CO_2} without a deflector is as high as 3.7%, which is double value of that with a deflector. Therefore, the ventilator mask without a deflector will lead to more CO_2 residue.

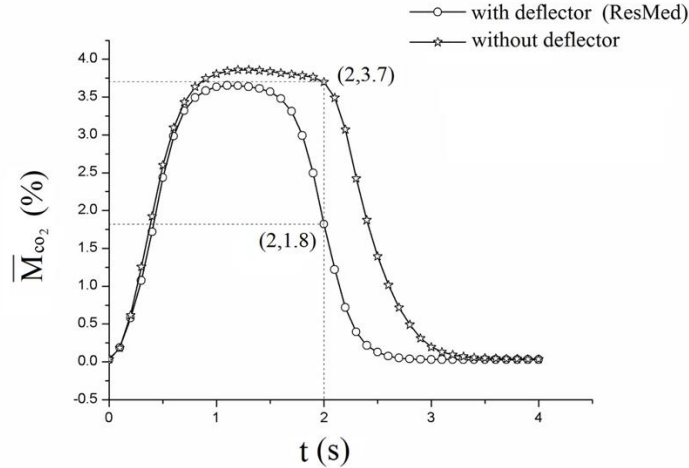


Figure 7: Plots of the averaged residual CO_2 concentration inside the nasal mask varying with time with/without deflector

3.3 Effects of the exhaust holes' positions on the averaged residual CO_2 concentration

To investigate the effects of the exhaust holes' positions on the \bar{M}_{CO_2} , the exhaust holes were redesigned on the top, both sides and the bottom of the ventilator mask, individually, with the same ventilating area. (Fig. 8A).

Figs. 8B and 8C are the plots of the velocity vector at the end time of expiratory ($t=2.0$ s), showing that: 1) When the exhaust holes are located at the top, most of the inlet air flows towards the top, leading to the lower velocity around the whole mask; 2) When the exhaust holes are located on both sides, the inlet air flows towards both sides, leading to the high velocity in the middle area of the mask and the formation of a low velocity vortex area in front of the nostrils; 3) When the exhaust holes are located at the bottom, the inlet air firstly flows towards the nose bridge, then flows towards the bottom. The air is quickly excreted from the exhaust holes, leading to a high velocity area below the nostrils and the formation of a low velocity vortex area in the distal of the exhaust holes.

Figs. 8D and 8E are the cloud maps of the residual CO_2 concentration at the end time of expiratory ($t=2.0$ s), showing that: 1) When the exhaust holes are located at the top, a great deal of CO_2 is trapped below the nostrils ($\bar{M}_{CO_2} \approx 4\%$); 2) When the exhaust holes are located on both sides, the \bar{M}_{CO_2} decreases to 50% ($\bar{M}_{CO_2} \approx 2\%$) except the CO_2 trapped near the wall of the mask; 3) When the exhaust holes are located at the bottom, the CO_2 is quickly excreted from the exhaust holes and the \bar{M}_{CO_2} decreases to 25% ($\bar{M}_{CO_2} \leq 1\%$).

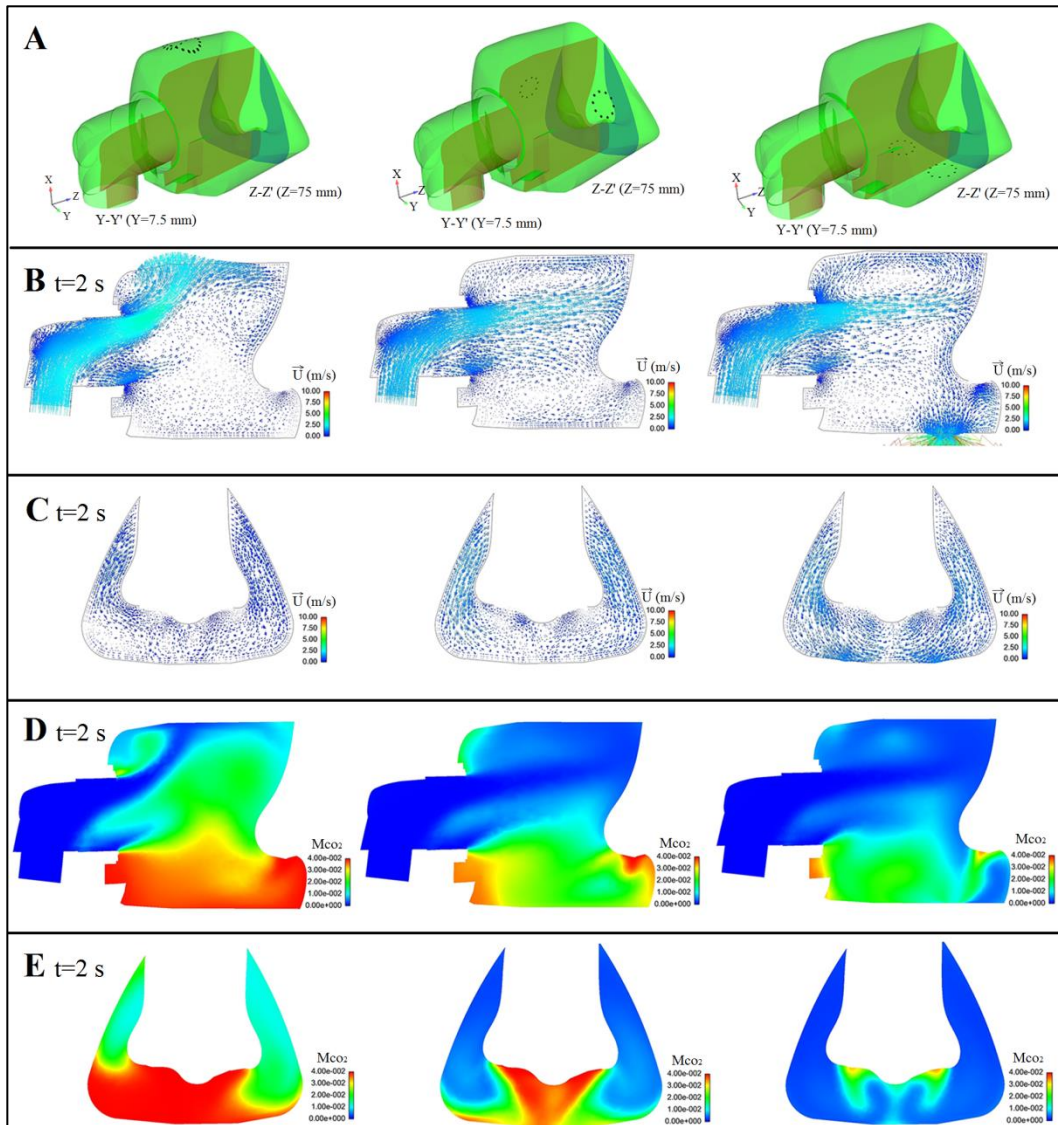


Figure 8: A. Different positions of the exhaust holes; B. The velocity vector plots on the crosssection Y-Y' at $t=2.0$ s; C. The velocity vector plots on the crosssection Z-Z' at $t=2.0$ s; D. The cloud maps of the residual CO_2 concentration on the crosssection Y-Y' at $t=2.0$ s; E. The cloud maps of the residual CO_2 concentration on the crosssection Z-Z' at $t=2.0$ s

Fig. 9 is the comparison analysis of the \bar{M}_{CO_2} varying with time inside the ventilator masks with different designs of the exhaust holes: 1) When the exhaust holes are located at the top, the peak value of the \bar{M}_{CO_2} is about 3.25%, which is lower than that of the Mirage SoftGel ventilator mask (3.65%). Meanwhile, the \bar{M}_{CO_2} at the end time of expiratory is about 2.1%, which is higher than that of the Mirage SoftGel ventilator mask

(1.8%); 2) When the exhaust holes are located on both sides, the \bar{M}_{CO_2} rises quickly to the peak value (about 3.7%) at $t=1.3$ s, then declines rapidly to the value of 1.4% at the end time of expiratory; 3) When the exhaust holes are located at the bottom, the \bar{M}_{CO_2} is lower than that of the other three designs in the whole expiratory phase and reaches the value of 0.7% at the end time of expiratory, which is significantly lower than that of the Mirage SoftGel ventilator mask (3.65%).

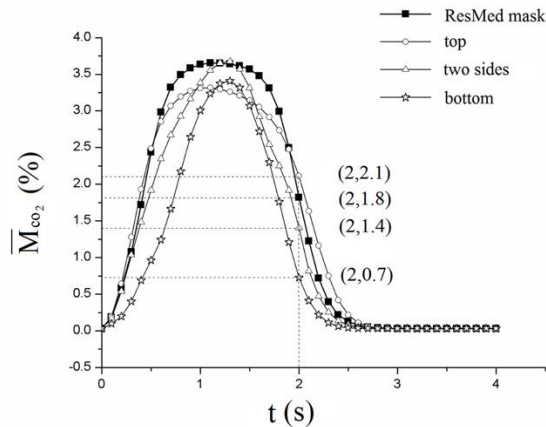


Figure 9: Plots of the averaged residual CO_2 concentration varying with time inside the nasal masks with different designs of the exhaust holes

4 Conclusion

With the air pollution as well as the changes in living and eating habits of people, OSAHS is becoming a more and more common respiratory disease, which may cause various cardiovascular and cerebrovascular diseases, and even lead to sudden death during sleep. Due to the trauma and easy relapse of surgical treatment, nowadays the commercially available household CPAP machine is commonly used to correct this sleep disorder. Ventilator mask is the most important component of this system and plays a key role in O_2 inhalation and CO_2 excretion. The less CO_2 residue, the better for the therapeutic effect. Therefore, the optimal design of the ventilator mask under near physiological condition is very important.

In present article, a 3D numerical model of the ventilator mask integrated with a volunteer's face was established and the nostrils boundary condition was considered, which were much closer to the reality. The results showed that the local averaged residual CO_2 concentration near the nostrils could reach to almost 4%, which was detrimental to the therapeutic effect. Therefore, the improved design of the ventilator mask was performed and found that by changing the position of the exhaust holes to the bottom, the local residual CO_2 concentration could decrease to 0.7%. Present study established a near physiological computational model and provided a new method for the individualized design of the commercial ventilator mask. In the future, a more realistic boundary

condition of human nostrils should be applied and a more reasonable method for the determination of carbon dioxide might be found.

Acknowledgment: We acknowledge the National Natural Science Foundation of China for supporting the project via the grant number 11472062 and 11002034.

References

- Buchanan, P.; Grunstein, R.** (2011): Positive airway pressure treatment for obstructive sleep apnea-hypopnea syndrome. *Principles and Practice of Sleep Medicine*, vol. 30, no. 12, pp. 1233-1249.
- Chen, H. X.** (2011): *Flowfield Simulation and Analysis Inside a CPAP Full Face Mask (Ph.D. Thesis)*. National Taiwan University of Science and Technology, China.
- Calay, R. K.; Kurujareon, J.; Holdo, A. E.** (2002): Numerical simulation of respiratory flow patterns within human lung. *Respiratory Physiology & Neurobiology*, vol. 130, no. 2, pp. 201.
- Chirapapaisan, N.; Likitgorn, T.; Pleumchitchom, M.; Sakiyalak, D.; Banhiran, W. et al.** (2016): Diurnal changes in retinal nerve fiber layer thickness with obstructive sleep apnea/hypopnea syndrome. *International Journal of Ophthalmology*, vol. 9, no. 7, pp. 979.
- De Vis, J. B.; Lu, H.; Ravi, H.; Hendrikse, J.; Liu, P.** (2017): Spatial distribution of flow and oxygenation in the cerebral venous drainage system. *Journal of Magnetic Resonance Imaging*, vol. 47, no. 4, pp. 1091-1098.
- George, D. L.; Daniel, R. P.** (2001): Inorganic compounds of Carbon, Nitrogen, and Oxygen. *Pattys Toxicology*, vol. 3, no. 5, pp. 607-730.
- Huang, T.; Wang, H.; Tan, J. X.** (2015): Effect of location and type of exhalation valve on carbon dioxide rebreathing during noninvasive positive pressure ventilation: An experimental study. *Zhonghua Wei Zhong Bing Ji Jiu Yi Xue*, vol. 27, no. 10, pp. 791-795.
- Kim, N. H.; Cho, N. H.; Yun, C. H.; Lee, S. K.; Yoon, D. W. et al.** (2013): Association of obstructive sleep apnea and glucose metabolism in subjects with or without obesity. *Diabetes Care*, vol. 36, no. 12, pp. 3909-3915.
- Korcarz, C. E.; Stein, J. H.; Peppard, P. E.; Young, T. B.; Barnet, J. H. et al.** (2014): Combined effects of sleep disordered breathing and metabolic syndrome on endothelial function: The wisconsin sleep cohort study. *Sleep*, vol. 37, no. 10, pp. 1707-1713.
- Li, K. K.** (2005): Surgical therapy for adult obstructive sleep apnea. *Sleep Medicine Reviews*, vol. 9, no. 3, pp. 201-209.
- Levitzky, M. G.** (2007): *Pulmonary Physiology*. McGraw-Hill, Health Professions Division, USA.
- Lofaso, F.; Brochard, L.; Touchard, D.; Hang, T.; Harf, A. et al.** (1995): Evaluation of carbon dioxide rebreathing during pressure support ventilation with airway management system (BiPAP) devices. *Chest*, vol. 108, no. 3, pp. 772-778.
- Liu, Y.; Lowe, A. A.; Fleetham, J. A.; Park, Y. C.** (2001): Cephalometric and physiologic predictors of the efficacy of an adjustable oral appliance for treating

obstructive sleep apnea. *American Journal of Orthodontics and Dentofacial Orthopedics*, vol. 120, no. 6, pp. 639-647.

Mcevoy, R. D.; Antic, N. A.; Heeley, E.; Luo, Y.; Ou, Q. et al. (2016): CPAP for prevention of cardiovascular events in obstructive sleep apnea. *New England Journal of Medicine*, vol. 375, no. 10, pp. 919-931.

Mediano, O.; Garcíarío, F.; Villasante, C. (2006): Comparison of carbon dioxide rebreathing during application of continuous positive airway pressure with 3 types of nasal mask. *Archivos De Bronconeumología*, vol. 42, no. 4, pp. 189-193.

Peng, B.; Wang, D.; Zhang, B. (2005): Effects of different expiratory valves on carbon dioxide repetitive respiration during noninvasive positive pressure ventilation. *Chinese Journal of Tuberculosis and Respiratory Diseases*, vol. 28, no. 12, pp. 875-876.

Rose, E. C.; Staats, R.; Virchow, C. J.; Jonas, I. E. (2002): Occlusal and skeletal effects of an oral appliance in the treatment of obstructive sleep apnea. *Chest*, vol. 122, no. 3, pp. 871-877.

Sun, X. W.; Li, Q. Y.; Shi, H. Y. (2016): A correlative study of OSAHS and hypercapnia. *Chest*, vol. 149, no. 4, pp. 572.

Shen, C. X.; Tan, M.; Song, X. L.; Xie, S. S.; Zhang, G. L. et al. (2017): Evaluation of the predictive value of red blood cell distribution width for onset of cerebral infarction in the patients with obstructive sleep apnea hypopnea syndrome. *Medicine*, vol. 96, no. 29.

Vecchierini, M. F.; Attali, V.; Collet, J. M.; d'Ortho, M. P.; El Chater, P. et al. (2016): A custom-made mandibular repositioning device for obstructive sleep apnoea-hypopnoea syndrome: The ORCADES study. *Sleep Medicine*, no. 19, pp. 131-140.

Wakayama, T.; Suzuki, M.; Tanuma, T. (2016): Effect of nasal obstruction on continuous positive airway pressure treatment: Computational fluid dynamics analyses. *Plos One*, vol. 11, no. 3.

Zhu, D. N.; Wang, T. H. (2013): *Physiology*. People's Medical Publishing House, Beijing.